PCCP

PAPER

View Article Online
View Journal

Cite this: DOI: 10.1039/c6cp04598g

Comparison of experimental and theoretical quantum-state-selected integral cross-sections for the $H_2O^+ + H_2$ (D_2) reactions in the collision energy range of 0.04–10.00 eV†

Hongwei Song,‡[a] Anyang Li,§[a] Hua Guo,*[a] Yuntao Xu,[b] Bo Xiong,[b] Yih-Chung Chang[b] and C. Y. Ng*[b]

Received 1st July 2016,
Accepted 21st July 2016

DOI: 10.1039/c6cp04598g

www.rsc.org/pccp

To understand the dynamics of H_3O^+ formation, we report a combined experimental–theoretical study of the rovibrationally state-selected ion–molecule reactions $H_2O^+(X^2B_1; v_1^+v_2^+v_3^+; N_{K_a^+K_c^+})$ + H_2 (D_2) → H_3O^+ (H_2DO^+) + H (D), where $(v_1^+v_2^+v_3^+)$ = (000), (020), and (100) and $N_{K_a^+K_c^+}$ = 0_{00}, 1_{11}, and 2_{11}. Both quantum dynamics and quasi-classical trajectory calculations were carried out on an accurate full-dimensional *ab initio* global potential energy surface, which involves nine degrees of freedom. The theoretical results are in good agreement with experimental measurements of the initial state specific integral cross-sections for the formation of H_3O^+ (H_2DO^+) and thus provide valuable insights into the surprising rotational enhancement and vibrational inhibition effects in these prototypical ion–molecule reactions that play a key role in the interstellar generation of OH and H_2O species.

I. Introduction

The formation of hydronium ions (H_3O^+) from the collision of water cations (H_2O^+) with hydrogen molecules (H_2) represents one of the most important ion–molecule reactions occurring in interstellar media.[1–3] As shown below, this reaction (R4) provides a critical link between two important oxygen containing cations (H_xO^+, x = 2 and 3) in space, where the hydroxyl radical (OH) and the water molecule (H_2O) can be formed by dissociative electron recombination with H_3O^+ cations.[1–3]

$$H^+ + O \rightarrow O^+ + H \quad (R1)$$

$$O^+ + H_2 \rightarrow OH^+ + H \quad (R2)$$

$$OH^+ + H_2 \rightarrow H_2O^+ + H \quad (R3)$$

$$H_2O^+ + H_2 \rightarrow H_3O^+ + H \quad (R4)$$

$$H_3O^+ + e \rightarrow OH + H_2 \quad (R5)$$

$$H_3O^+ + e \rightarrow H_2O + H \quad (R6)$$

Both the H_2O^+ and H_3O^+ cations have recently been detected in several interstellar environments by the Herschel space-based telescope,[4–6] firmly establishing their roles in astrochemistry. Given the importance of OH and H_2O and their anions in space,[3,7] understanding these reactions is highly desired. Previous chemical kinetic studies show that the titled reactions have gas-kinetic rate coefficients, indicative of a reaction pathway without a potential barrier.[8–16]

In addition to astrophysical importance, (R4) also provides an ideal platform to study mode-specific reactivity in ion–molecule reactions. Using a novel quantum-state-selection scheme[17–22] based on the pulsed field ionization (PFI) of high-n ($n > 100$) Rydberg H_2O molecules populated by tunable vacuum ultraviolet (VUV) laser excitation, the integral cross-sections for the rovibrationally state-selected ion–molecule reaction (R4) [$\sigma(H_3O^+: v_1^+v_2^+v_3^+; N_{K_a^+K_c^+})$] in the center-of-mass kinetic energy (E_{cm}) range of 0.03–10.00 eV have been measured.[19,20,22] The application of the newly developed VUV laser PFI-photoion (PFI-PI) state-selected ion–molecule reaction scheme has not only made possible the preparation of $H_2O^+(X^2B_1)$ in single rovibrational states, but also achieved high kinetic energy resolution, allowing the examination of rotational and vibrational quantum-state effects for reaction (R4) down to thermal energies (≈30 meV).[19,20,22] Such a precise control of initial reactant internal excitation and collision energy is unprecedented and as a result these experimental data provide valuable benchmarks for theoretical studies of quantum state resolved reactivity in this prototypical ion–molecule reaction.

[a] Department of Chemistry and Chemical Biology, University of New Mexico, Albuquerque, NM 87131, USA. E-mail: hguo@unm.edu
[b] Department of Chemistry, University of California, Davis, CA 95616, USA. E-mail: cyng@ucdavis.edu

† Electronic supplementary information (ESI) available. See DOI: 10.1039/c6cp04598g

‡ Present address: State Key Laboratory of Magnetic Resonance and Atomic and Molecular Physics, Wuhan Institute of Physics and Mathematics, Chinese Academy of Sciences, Wuhan 430071, China.

§ Present address: College of Chemistry and Materials Science, Northwest University, Xi'an, 710069, China.

Integral cross-sectional measurements reveal strong rotational enhancement and vibrational inhibition effects for these reactions.[19,20,22,23] The signature of the rotational enhancement was also found to manifest in the temperature dependence of the rate coefficient of the titled reaction.[16] An exothermic, barrierless complex-forming reaction typically depends only weakly on the internal excitation of the reactant[24,25] and thus the observed strong dependence of reactivity on reactant internal excitations, particularly at low E_{cm} values, was a surprise.[19,20,22,23] We have attributed the observed rotational enhancement effect in (R4) to the strong coupling of the reaction coordinate at the submerged saddle point with a rotational mode of H_2O^+,[26] based on the recently proposed Sudden Vector Projection model.[27] Interestingly, a similar rotational enhancement effect was found in the $OH^+ + H_2$ reaction (R3),[28] which has a similar potential energy profile to a submerged saddle region.[29] Both quantum dynamic (QD) and quasi-classical trajectory (QCT) studies have been performed for (R3) on a global *ab initio* potential energy surface (PES),[28] and the results are found to be in agreement with the measured rate coefficients and kinetic isotope effects.[30]

To gain further insights into the reaction dynamics of (R4), we report here a detailed study on (R4) and its deuterated isotopologue:

$$H_2O^+ + D_2 \rightarrow H_2DO^+ + D \qquad (R4')$$

with a combined theoretical–experimental approach. For the reactant H_2O^+ ion in its ground ro-vibrational state, (R4) and (R4′) are exothermic by 1.68 and 1.72 eV, respectively.[31] To facilitate the theoretical studies, an accurate global PES including all nine internal degrees of freedom has been constructed for the reaction dynamics study of reactions (R4) and (R4′).[26] The high fidelity fit to about 81 000 high-level *ab initio* points was achieved using the recently proposed permutation-invariant polynomial neural network method.[32,33] The PES suggests a barrierless reaction pathway, consistent with the monotonically decaying profile of the $\sigma(H_3O^+: v_1^+v_2^+v_3^+; N_{K_a^+K_c^+})$ curves measured as a function of E_{cm}.[19,20,22,23] In this work, we report extensive QD and QCT predictions of the initial state selected integral cross-sections for reactions (R4) and (R4′) at E_{cm} = 0.04–1.00 eV obtained using this full-dimensional global PES.[26] The QD calculations are particularly demanding because of the huge size of basis/points and very long propagation time. In addition, we also present new experimental data on the ro-vibrational state-selective integral cross-sections for (R4′) [$\sigma(H_2DO^+: v_1^+v_2^+v_3^+; N_{K_a^+K_c^+})$]. The comparison of the theoretical predictions with experimental measurements presented here and in our earlier publications sheds valuable light on the reaction dynamics.[19,20,22]

II. Methods

The $\sigma(H_3O^+: v_1^+v_2^+v_3^+; N_{K_a^+K_c^+})$ and $\sigma(H_2DO^+: v_1^+v_2^+v_3^+; N_{K_a^+K_c^+})$ measurements for reactions (R4) and (R4′) were conducted by employing the VUV laser PFI-PI state-selected ion–molecule reaction apparatus, which has been described in detail in ref. 18 and 20. Briefly, the apparatus consists of a VUV laser PFI-PI ion source for the preparation of a quantum-state-selected $H_2O^+(X^2B_1; v_1^+v_2^+v_3^+; N_{K_a^+K_c^+})$ ion beam, a dual set of radio frequency octopole ion guides for confining and guiding the reactant and product ions, a reactant gas cell, where the $H_2O^+ + H_2$ (D_2) reactions occur, and a quadrupole mass spectrometer for the detection of reactant and product ions. Tunable VUV laser radiation was generated by four-wave sum-frequency mixing schemes using Xe gas as the nonlinear medium for the preparation of rovibrationally selected reactant $H_2O^+(X^2B_1)$ ions, covering the vibrational states of $(v_1^+v_2^+v_3^+)$ = (000), (020), and (100), and the rotational levels of $N_{K_a^+K_c^+}$ = 0_{00}, 1_{11}, and 2_{11}. The reactant $H_2O^+(X^2B_1; v_1^+v_2^+v_3^+; N_{K_a^+K_c^+})$ PFI-PI beam thus prepared achieves a narrow laboratory kinetic energy (E_{lab}) spread ($\Delta E_{lab} = \pm 0.05$ eV).[19,22] For all experimental integral cross-sections presented here, the run-to-run uncertainties were 10%, whereas the systematic errors in the experimental absolute cross-sections are estimated to be 50%.

The QD calculations were performed with a reduced seven-dimensional Hamiltonian,[34–36] in which the two non-reactive O–H bonds are fixed for the penta-atomic reaction AB + CDE defined in Jacobi coordinates, as shown in Fig. 1. For a given total angular momentum (J_{tot}), the Hamiltonian can be written as ($\hbar$ = 1 hereafter)

$$\hat{H} = -\frac{1}{2\mu_R}\frac{\partial^2}{\partial R^2} + \hat{h}_1(r_1) + \frac{(\hat{J}_{tot} - \hat{J})^2}{2\mu_R R^2} + \frac{\hat{j}_1^2}{2\mu_1 r_1^2} + \frac{\hat{l}_2^2}{2\mu_2 r_{20}^2} + \frac{\hat{j}_3^2}{2\mu_3 r_{30}^2} + \hat{V}(R, r_1, r_{20}, r_{30}, \theta_1, \theta_2, \theta_3, \varphi_1, \varphi_2) - V^{ref}(r_1), \qquad (1)$$

where R is the distance between the centers of mass (COMs) of AB and E-CD, r_1 is the bond distance of AB, r_3 is the bond distance of CD and r_2 is the distance from E to the COM of CD, which are fixed at $r_{30} = 1.8881a_0$ and $r_{20} = 1.9281a_0$, respectively. Since the O atom (D) is much heavier than the H atom (C and E), this is approximately equivalent to fixing the two nonreactive OH bonds. The corresponding reduced mass values are given by μ_R, μ_1, μ_2, and μ_3. $\hat{j}_3$ is the rotational angular momentum operator of CD and $\hat{l}_2$ is the orbital angular momentum operator of atom E with respect to CD. $\hat{j}_{23}$ is the angular momentum operator of CDE, which is the sum of $\hat{j}_3$ and $\hat{l}_2$. $\hat{j}_1$ is the rotational angular momentum operator of AB. $\hat{J}$ is the sum of $\hat{j}_1$ and $\hat{j}_{23}$. $\hat{J}_{tot}$ is the total angular momentum operator of the system. $\hat{h}_1(r_1)$ is

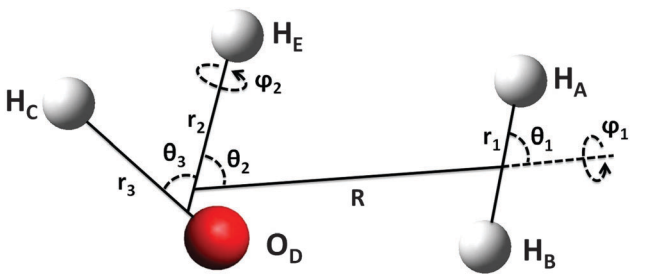

Fig. 1 The nine-dimensional Jacobi coordinates of the AB + CDE system.

the one-dimensional (1D) reference Hamiltonian, which is defined as

$$\hat{h}_1(r_1) = -\frac{1}{2\mu_1}\frac{\partial^2}{\partial {r_1}^2} + V^{\mathrm{ref}}(r_1), \qquad (2)$$

where $V^{\mathrm{ref}}(r_1)$ is the corresponding 1D reference potential.

As detailed in the ESI,† the parity-adapted wave function was expanded in terms of the body-fixed ro-vibrational basis functions, within the centrifugal-sudden (CS) approximation.[37,38] Initial wave packets corresponding to different ro-vibrational states of the H_2O^+ reactant were launched from the reactant asymptote and propagated on the PES using the split-operator method.[39] The propagation was accelerated by using a massively parallel implementation in computing the action of the Hamiltonian on the wave function. The total reaction probabilities were obtained using a flux method and the final integral cross-sections were obtained by summing over all partial waves. The parameters used in the QD calculations are given in the ESI.†

Standard QCT calculations were carried out on the same PES, using VENUS.[40,41] The H_2O^+ reactant was prepared by fixed normal mode energy sampling of the initial conditions. Since the rotational excited states cannot be assigned using rotational quantum numbers in the QCT calculation, the H_2O^+ rotational excitation was approximated by fixing the rotational energy in each axis with $kT/2$. The temperatures 54 and 125 K correspond to the rotational excited states $N_{K_a{}^+K_c{}^+} = {}^{1}1_1$, and 2_{11} with the excited energies of 37.45 and 86.82 cm^{-1}, respectively The ro-vibrational state of the H_2 reactant was sampled from a Boltzmann distribution at the experiment temperature (298 K) using the classical action-angle variables. Further details of the QCT calculations can also be found in the ESI.†

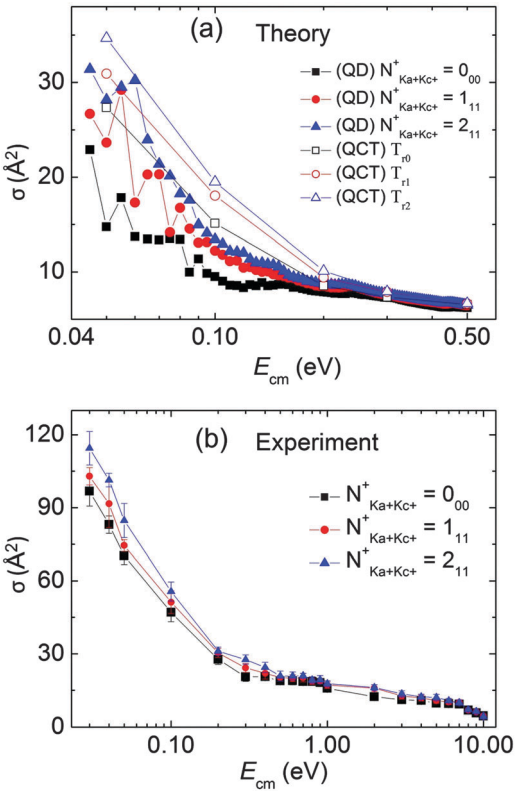

Fig. 2 (a) Theoretical QD and QCT $\sigma(H_3O^+$: 000; 0_{00}, 1_{11} and $2_{11})$ values in $Å^2$ calculated at E_{cm} = 0.04–0.50 eV. For QCT calculations, the 0_{00}, 1_{11} and 2_{11} energies are specified by the rotational temperatures, T_{r0}, T_{r1}, and T_{r2}, respectively. (b) Experimental $\sigma(H_3O^+$: 000; 0_{00}, 1_{11} and $2_{11})$ values in $Å^2$ obtained at E_{cm} = 0.03–10.00 eV by using the VUV laser PFI-PI state-selection method.

III. Results and discussion

Fig. 2(a) depicts the QD $\sigma(H_3O^+$: ${\nu_1}^+{\nu_2}^+{\nu_3}^+$; $N_{K_a{}^+K_c{}^+})$ curves for (R4) with $({\nu_1}^+{\nu_2}^+{\nu_3}^+)$ = (000), $N_{K_a{}^+K_c{}^+} = {}^{0}0_{00}$, 1_{11} and 2_{11}, and E_{cm} = 0.04–0.50 eV. Here, the reactant H_2 is set in its ground ro-vibrational state. For reactant H_2O^+ in the asymmetric top designation, the 1_{11} and 2_{11} states correspond to the 2nd and 6th excited rotational states, respectively. In QD calculations, the reactant rotational levels are solved quantum mechanically, so that these initial rotational states are well specified. The experimental $\sigma(H_3O^+$: 000; 0_{00}, 1_{11} and $2_{11})$ curves[23] observed by employing the VUV laser PFI-PI method in the E_{cm} range of 0.03–10.00 eV are shown in Fig. 2(b) for comparison with the QD and QCT calculations of Fig. 2(a). As reported previously,[19,20,23] the experimental cross-sections in Fig. 2(b) clearly reveal a rotational enhancement effect for (R4), *i.e.*, the integral cross-section becomes higher for a higher rotational excitation at $E_{cm} < 0.50$ eV.

The QD $\sigma(H_3O^+$: 000; 0_{00}, 1_{11} and $2_{11})$ curves of Fig. 2(a) exhibit strong oscillations at low $E_{cm} < 0.20$ eV, which can be attributed to quantum resonances. Since these oscillations for different rotational states are not in phase, they are expected to be smoothened out for H_3O^+ ions produced with a distribution of rotational states. Despite the strong oscillations, the QD results clearly show $\sigma(H_3O^+$: 000; $0_{00}) < \sigma(H_3O^+$: 000; $1_{11}) < \sigma(H_3O^+$: 000; $2_{11})$, which is consistent with the experimentally observed rotational enhancement effect. The quantum oscillations are not observed in the experimental curves in Fig. 2(b). As pointed out previously,[20,42] since the ΔE_{cm} spread in the experiment is largely caused by the thermal motion of H_2 in the reaction gas cell at 298 K, the ΔE_{cm} values are comparable or greater than the widths of the predicted quantum oscillations, thus unresolved in the present study. It is also possible that these oscillations are due to artifacts of the CS approximation.[37,38]

In the QCT calculations, the reactant H_2O^+ was prepared in fixed normal mode energy sampling with given quantum numbers of vibrational states. However, the quantum rotational states cannot be precisely defined and thus the three 0_{00}, 1_{11} and 2_{11} rotational states were approximated by setting the rotational temperatures at T_{r0} = 0, T_{r1} = 54, and T_{r2} = 125 K, which correspond to energies of 0.00, 37.45 and 86.82 cm^{-1} for the three rotational levels. The QCT $\sigma(H_3O^+$: 000; T_{r0}, T_{r1} and $T_{r2})$ curves obtained at selected E_{cm} values are also depicted in Fig. 2(a). As expected, the oscillations observed in the QD curves are absent in the QCT curves. The profiles of the QCT curves of Fig. 2(a) are found to be similar to those of the experimental curves[19,20,23] shown in Fig. 2(b), which decay rapidly as E_{cm} is increased. The QCT $\sigma(H_3O^+$: 000; T_{r0}, T_{r1} and $T_{r2})$ values appear

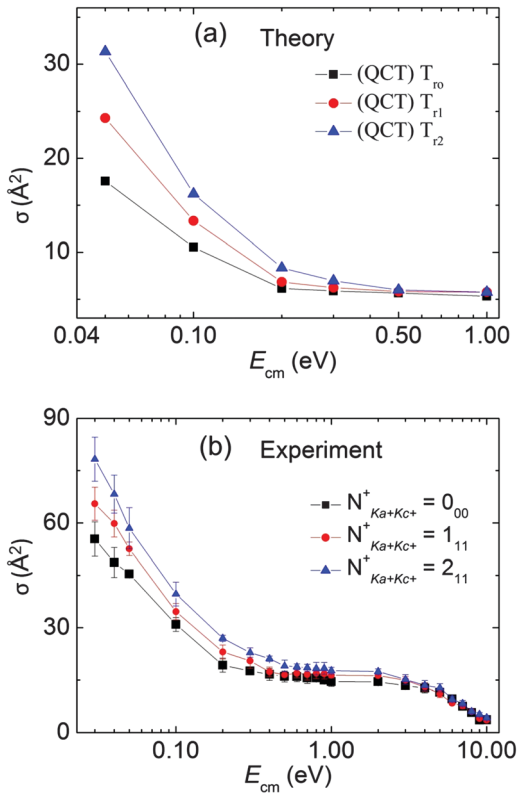

Fig. 3 (a) Theoretical QCT $\sigma(H_2DO^+$: 000; T_{t0}, T_{r1} and $T_{r2})$ values in Å^2 calculated at E_{cm} = 0.05–1.00 eV. (b) Experimental $\sigma(H_2DO^+$: 000; 0_{00}, 1_{11} and $2_{11})$ values in Å^2 measured at E_{cm} = 0.03–10.00 eV by using the VUV laser PFI-PI state-selection method.

to be higher than the QD values at the same E_{cm} value. This can presumably be attributed to zero-point energy (ZPE) leakage, which is known to be an intrinsic defect in the QCT methodology. Nevertheless, the QCT $\sigma(H_3O^+$: 000; T_{r0}, T_{r1} and $T_{r2})$ curves are in qualitative agreement with the experimental $\sigma(H_3O^+$: 000; 0_{00}, 1_{11} and $2_{11})$ curves,[23] showing a strong rotational enhancement effect at E_{cm} = 0.04–0.20 eV.

The QCT $\sigma(H_2DO^+$: 000; T_{r0}, T_{r1} and $T_{r2})$ curves for (R4′) calculated at E_{cm} = 0.05–1.00 eV are depicted in Fig. 3(a). The experimental $\sigma(H_2DO^+$: 000; 0_{00}, 1_{11} and $2_{11})$ curves[19,20] measured at E_{cm} = 0.03–10.00 eV are shown in Fig. 3(b) for comparison with the QCT results of Fig. 3(a). The QCT $\sigma(H_2DO^+$: 000; T_{r0}, T_{r1} and $T_{r2})$ values are also found to have similar E_{cm} and rotational dependencies to those observed for the experimental $\sigma(H_2DO^+$: 000; 0_{00}, 1_{11} and $2_{11})$ curves, indicating that the rotational enhancement effect for (R4′) observed at low $E_{cm} < 0.50$ eV is also predicted by the QCT calculation. The cross-section ratios, $\sigma(H_2DO^+$: 000; $0_{00}) : \sigma(H_2DO^+$: 000; $1_{11}) : \sigma(H_2DO^+$: 000; $2_{11})$ of Fig. 3(b) appear to be larger than the ratios, $\sigma(H_3O^+$: 000; $0_{00}) : \sigma(H_3O^+$: 000; $1_{11}) : \sigma(H_3O^+$: 000; $2_{11})$, shown in Fig. 2(b). This greater rotational enhancement effect observed for (R4′) than that for (R4) is also consistent with the QCT predictions.

The origin of the rotational enhancement effect for the titled reactions was rationalized previously by Li *et al.* based on the PES of the $H_2O^+ + H_2$ reaction system obtained by high-level *ab initio* quantum calculations.[23] These calculations show that the long range charge and dipole–induced-multipole interactions between the ion and neutral reactants play an important role in the reaction dynamics. The long range forces govern H_2 to approach perpendicularly toward an H end of H_2O^+ to form a weak ion–neutral complex. The rotational enhancement of the H_2O^+ reactivity was attributed to the reorientation of H_2O^+ facilitated by rotational excitation to make the O end of H_2O^+ close to H_2 to form the transition structure prior to entering the strong chemical complex that leads to the formation of products $H_3O^+ + H$. A slight, submerged potential barrier was predicted at the transition structure, which represents the bottleneck and was found to be a key feature along the reaction pathway. It was shown using the Sudden Vector Projection model[27] that the rotational modes of the H_2O^+ reactant are strongly coupled with the reaction coordinate at this saddle point, leading to an enhancement of reactivity.[26] The theoretical cross-sections confirm the rationalization of the reaction mechanism presented previously.

To avoid the nearly prohibitive costs of QD calculations, we have only employed the QCT method to study the reactant vibrational effect. Since the QCT model has successfully predicted the rotational enhancement effect for (R4) and (R4′), the combination of state-selective experimental measurements and QCT calculations is also expected to provide valuable dynamical insights into the vibrational effects of these reactions.

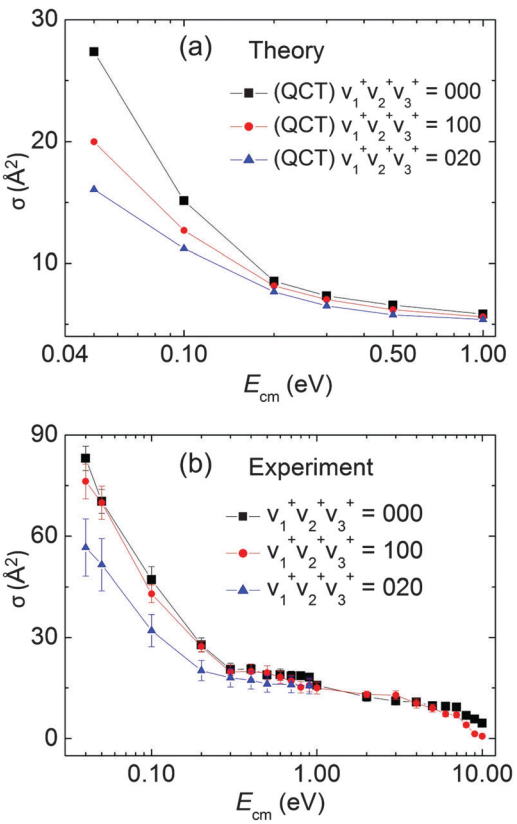

Fig. 4 (a) Theoretical QCT $\sigma(H_3O^+$: 000, 100, and 020; $T_{r0})$ values in Å^2 calculated at E_{cm} = 0.05–1.00 eV. (a) Experimental $\sigma(H_3O^+$: 000, 100, and 020; $0_{00})$ values in Å^2 measured at E_{cm} = 0.04–10.00 eV by using the VUV laser PFI-PI state-selection method.

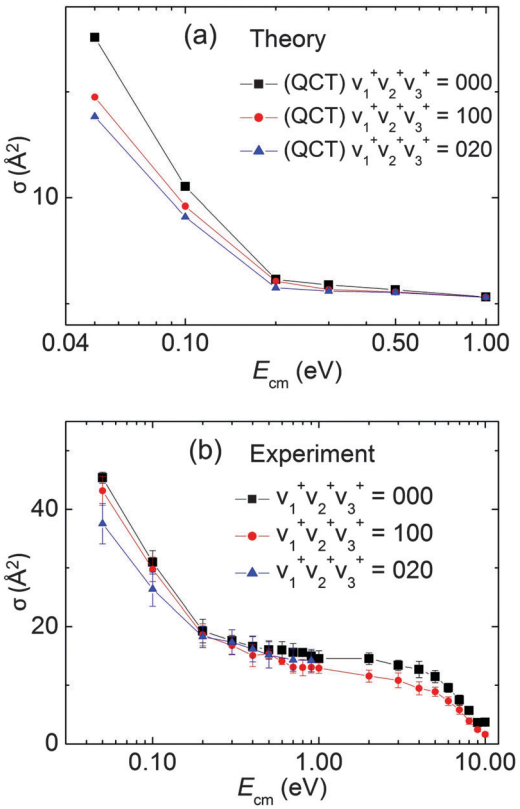

Fig. 5 (a) Theoretical QCT $\sigma(H_2DO^+$: 000, 100, and 020; $T_{r0})$ values in Å^2 calculated at E_{cm} = 0.05–1.00 eV. (b) Experimental $\sigma(H_2DO^+$: 000, 100, and 020; $0_{00})$ values in Å^2 measured at E_{cm} = 0.04–10.00 eV by using the VUV laser PFI-PI state-selection method.

The QCT $\sigma(H_3O^+$: $v_1^+v_2^+v_3^+$; $T_{r0})$ [QCT $\sigma(H_2DO^+$: $v_1^+v_2^+v_3^+$; $T_{r0})$] curves calculated at $v_1^+v_2^+v_3^+$ = (000), (020), and (100) and E_{cm} = 0.05–1.00 eV are plotted in Fig. 4(a) [Fig. 5(a)]. As shown in these figures, the QCT calculations predict a strong vibrational inhibition effect on H_2O^+ reactivity at low E_{cm} = 0.05–0.20 eV, when H_2O^+ is excited to the (020) and (100) vibrational states. The QCT cross-sections for the (000), (020), and (100) vibrational states are predicted to be close at $E_{cm} \approx$ 0.20–1.00 eV. The experimental $\sigma(H_3O^+$: $v_1^+v_2^+v_3^+$; $0_{00})$ [$\sigma(H_2DO^+$: $v_1^+v_2^+v_3^+$; $0_{00})$] curves measured at $v_1^+v_2^+v_3^+$ = (000), (020), and (100) and E_{cm} = 0.04–10.00 eV are plotted in Fig. 4(b) [Fig. 5(b)], showing that the excitation of the (020) mode results in the largest suppression of the reaction cross-sections at E_{cm} below 0.20 eV.[20] Although the observed experimental trends, $\sigma(H_3O^+$: 020; $0_{00}) < \sigma(H_3O^+$: 100; $0_{00}) < \sigma(H_3O^+$: 000; $0_{00})$ [$\sigma(H_2DO^+$: 020; $0_{00}) < \sigma(H_2DO^+$: 100; $0_{00}) < \sigma(H_2DO^+$: 000; $0_{00})$], for (R4) [(R4′)], are in qualitative agreement with the QCT results of Fig. 4(a) [Fig. 5(a)], the experimental $\sigma(H_3O^+$: 100; $0_{00})$ [$\sigma(H_2DO^+$: 100; $0_{00})$] values are nearly the same as the $\sigma(H_3O^+$: 000; $0_{00})$ [$\sigma(H_2DO^+$: 000; $0_{00})$] values after taking into account experimental uncertainties. That is, the inhibition effect for the (100) state observed in the present experiment is small at E_{cm} below 0.20 eV. However, at E_{cm} = 1.00–10.00 eV, where the QCT calculations were not made, the experimental measurements show clearly that $\sigma(H_3O^+$: 100; $0_{00})$ is significantly lower than $\sigma(H_3O^+$: 000; $0_{00})$, indicative of a strong inhibition for the (100) state.

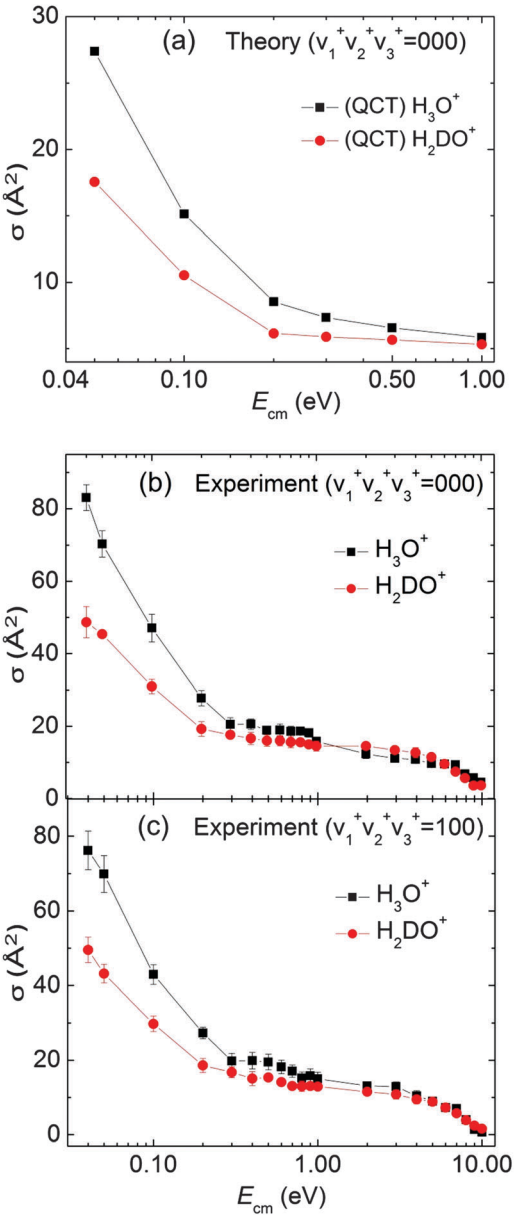

Fig. 6 (a) Theoretical QCT $\sigma(H_3O^+$: 000; $T_{r0})$ and QCT $\sigma(H_2DO^+$: 000; $T_{r0})$ values in Å^2 calculated at E_{cm} = 0.04–1.00 eV. (b) Experimental $\sigma(H_3O^+$: 000; $0_{00})$ and $\sigma(H_2DO^+$: 000; $0_{00})$ values in Å^2 measured at E_{cm} = 0.04–10.00 eV by using the VUV laser PFI-PI state-selection method. (c) Experimental $\sigma(H_3O^+$: 100; $0_{00})$ and $\sigma(H_2DO^+$: 100; $0_{00})$ values in Å^2 measured at E_{cm} = 0.04–10.00 eV by using the VUV laser PFI-PI state-selection method.

Considering that the frequency of 3211 cm^{-1} for the (100) mode is only 450 cm^{-1} higher than that of 2771 cm^{-1} for the (020) mode,[20] the greater vibrational inhibition observed for the (020) bending mode than the (100) stretching mode is intriguing. The most important long-range interactions are due to charge-quadrupole and charge-induced dipole interactions, which are proportional to r^{-3} and r^{-4}, respectively, where r is the separation between the center-of-charge of the H_2O^+ ion and the center-of-charge of the H_2 molecule. Since the bending vibration has the largest effect on the center-of-charge

of H_2O^+, the observed inhibition by the (020) excitation may result from the effect of the bending excitation on the center-of-charge of reactant H_2O^+, while the symmetric stretching mode is expected to have little effect on the center-of-charge.

Fig. 6(a) compares the QCT $\sigma(H_3O^+: 000; T_{r0})$ with the QCT $\sigma(H_2DO^+: 000; T_{r0})$ curves calculated at E_{cm} = 0.04–1.00 eV, showing a pronounced isotopic effect at E_{cm} below 0.30 eV with the cross-section for the D_2 reaction significantly lower than that for the H_2 reaction. As the E_{cm} is increased, the difference between the cross-sections for the H_2 and D_2 reactions becomes less. The comparison of the experimental $\sigma(H_3O^+: 000; 0_{00})$ and $\sigma(H_2DO^+: 000; 0_{00})$ [$\sigma(H_2DO^+: 100; 0_{00})$ and $\sigma(H_2DO^+: 100; 0_{00})$] curves[19,20,23] is shown in Fig. 6(b) [Fig. 6(c)]. These comparisons in Fig. 6(a)–(c) show that the QCT calculations are in qualitative agreement with the experimental observation of the isotopic effect, indicating that the $\sigma(H_3O^+: {\nu_1}^+{\nu_2}^+{\nu_3}^+; 0_{00})$ values are significantly larger than $\sigma(H_2DO^+: {\nu_1}^+{\nu_2}^+{\nu_3}^+; 0_{00})$ at E_{cm} < 1.00 eV with ${\nu_1}^+{\nu_2}^+{\nu_3}^+$ = 000 and 100.

IV. Summary

The experimental and theoretical results presented above greatly advance our understanding of these astrochemically important ion–molecule reactions with unprecedented detail. The QD and QCT studies of both (R4) and (R4′) on an accurate PES reproduced semi-quantitatively the experimentally measured integral cross-sections over a large energy range and the surprising rotational enhancement effect. The theoretical results also offer a more in-depth understanding of the mode specificity. The agreement between the QD and QCT results suggest that the dynamics of the title reactions are fast and direct, and as a result can be described with reasonable accuracy using QCT. Indeed, the QCT predictions of the vibrational inhibition and isotope effects are in excellent agreement with experimental measurements.

Although the relative values and profiles for the $\sigma(H_3O^+: {\nu_1}^+{\nu_2}^+{\nu_3}^+; N_{K_a{}^+K_c{}^+})$ and $\sigma(H_2DO^+: {\nu_1}^+{\nu_2}^+{\nu_3}^+; N_{K_a{}^+K_c{}^+})$ curves obtained by the theoretical calculations and experimental measurements presented here are in qualitative agreement, the absolute values for the experimental cross-sections are found to be about a factor of two higher than the theoretical cross-sections. Due to the difficulties in calibrating the absolute cross-section scale, the experimental absolute cross-section values presented here have some uncertainties. Similarly, the ZPE leakage effect in the QCT calculations and neglect of the Coriolis coupling in the QD calculations also render the theoretical cross-sections with large uncertainties. Thus, the comparison of the relative cross-sections as shown above is expected to be more meaningful than the comparison of the absolute values. It is interesting to note that significant translational, rotational, and vibrational as well as isotopic effects for the titled reactions are all observed at E_{cm} below 0.50 eV. The QD cross-section curves calculated for the reactant H_2O^+ formed in single rotational states reveal pronounced oscillations, which might be attributable to quantum resonances.

Acknowledgements

This material is based upon work supported by the National Science Foundation under CHE-1462172 to CYN and the Department of Energy under DE-FG02-05ER15694 to HG.

References

1 E. Herbst and W. Klemperer, *Astrophys. J.*, 1973, **185**, 505.
2 W. D. Watson, *Acc. Chem. Res.*, 1977, **10**, 221.
3 H. David, M. J. Kaufman, D. Neufeld, M. Wolfire and J. R. Goicoechea, *Astrophys. J.*, 2012, **754**, 105.
4 D. A. Neufeld, J. R. Goicoechea, P. Sonnentrucker, J. H. Black, J. Pearson, S. Yu, T. G. Phillips, D. C. Lis, M. De Luca, E. Herbst, P. Rimmer, M. Gerin, T. A. Bell, F. Boulanger, J. Cernicharo, A. Coutens, E. Dartois, M. Kazmierczak, P. Encrenaz, E. Falgarone, T. R. Geballe, T. Giesen, B. Godard, P. F. Goldsmith, C. Gry, H. Gupta, P. Hennebelle, P. Hily-Blant, C. Joblin, R. Kołos, J. Krełowski, J. Martín-Pintado, K. M. Menten, R. Monje, B. Mookerjea, M. Perault, C. Persson, R. Plume, M. Salez, S. Schlemmer, M. Schmidt, J. Stutzki, D. Teyssier, C. Vastel, A. Cros, K. Klein, A. Lorenzani, S. Philipp, L. A. Samoska, R. Shipman, A. G. G. M. Tielens, R. Szczerba and J. Zmuidzinas, *Astron. Astrophys.*, 2010, **521**, L10.
5 M. Gerin, M. De Luca, J. Black, J. R. Goicoechea, E. Herbst, D. A. Neufeld, E. Falgarone, B. Godard, J. C. Pearson, D. C. Lis, T. G. Phillips, T. A. Bell, P. Sonnentrucker, F. Boulanger, J. Cernicharo, A. Coutens, E. Dartois, P. Encrenaz, T. Giesen, P. F. Goldsmith, H. Gupta, C. Gry, P. Hennebelle, P. Hily-Blant, C. Joblin, M. Kazmierczak, R. Kolos, J. Krelowski, J. Martin-Pintado, R. Monje, B. Mookerjea, M. Perault, C. Persson, R. Plume, P. B. Rimmer, M. Salez, M. Schmidt, J. Stutzki, D. Teyssier, C. Vastel, S. Yu, A. Contursi, K. Menten, T. Geballe, S. Schlemmer, R. Shipman, A. G. G. M. Tielens, S. Philipp-May, A. Cros, J. Zmuidzinas, L. A. Samoska, K. Klein and A. Lorenzani, *Astron. Astrophys.*, 2010, **518**, L110.
6 E. González-Alfonso, J. Fischer, S. Bruderer, H. S. P. Müller, J. Graciá-Carpio, E. Sturm, D. Lutz, A. Poglitsch, H. Feuchtgruber, S. Veilleux, A. Contursi, A. Sternberg, S. Hailey-Dunsheath, A. Verma, N. Christopher, R. Davies, R. Genzel and L. Tacconi, *Astron. Astrophys.*, 2013, **550**, A25.
7 T. L. Williams, N. G. Adams, L. M. Babcock, C. R. Herd and M. Geoghegan, *Mon. Not. R. Astron. Soc.*, 1996, **282**, 413.
8 D. A. Kubose and W. H. Hamill, *J. Am. Chem. Soc.*, 1963, **85**, 125.
9 F. C. Fehsenfeld, A. L. Schmeltekopf and E. E. Ferguson, *J. Chem. Phys.*, 1967, **46**, 2802.
10 A. G. Harrison and J. C. J. Thynne, *Trans. Faraday Soc.*, 1968, **64**, 945.
11 J. K. Kim, L. P. Theard and W. T. Huntress, *J. Chem. Phys.*, 1975, **62**, 45.
12 I. Dotan, W. Lindinger, B. Rowe, D. W. Fahey, F. C. Fehsenfeld and D. L. Albritton, *Chem. Phys. Lett.*, 1980, **72**, 67.
13 A. B. Rakshit and P. Warneck, *J. Chem. Soc., Faraday Trans. 2*, 1980, **76**, 1084.
14 A. B. Rakshit and P. Warneck, *J. Chem. Phys.*, 1981, **74**, 2853.

15 J. D. C. Jones, K. Birkinshaw and N. D. Twiddy, *Chem. Phys. Lett.*, 1981, **77**, 484.
16 S. G. Ard, A. Li, O. Martinez, N. S. Shuman, A. A. Viggiano and H. Guo, *J. Phys. Chem. A*, 2014, **118**, 11485.
17 Y. C. Chang, H. Xu, Y. Xu, Z. Lu, Y.-H. Chiu, D. J. Levandier and C. Y. Ng, *J. Chem. Phys.*, 2011, **134**, 201105.
18 Y. C. Chang, Y. Xu, Z. Lu, H. Xu and C. Y. Ng, *J. Chem. Phys.*, 2012, **137**, 104202.
19 Y. Xu, B. Xiong, Y. C. Chang and C. Y. Ng, *J. Chem. Phys.*, 2012, **137**, 241101.
20 Y. Xu, B. Xiong, Y. C. Chang and C. Y. Ng, *J. Chem. Phys.*, 2013, **139**, 024203.
21 Y. Xu, Y. C. Chang, Z. Lu and C. Y. Ng, *Astrophys. J.*, 2013, **769**, 72.
22 C.-Y. Ng, *Annu. Rev. Phys. Chem.*, 2014, **65**, 197.
23 A. Li, Y. Li, H. Guo, K.-C. Lau, Y. Xu, B. Xiong, Y.-C. Chang and C. Y. Ng, *J. Chem. Phys.*, 2014, **140**, 011102.
24 J. Troe, *J. Chem. Soc., Faraday Trans.*, 1994, **90**, 2303.
25 H. Guo, *Int. Rev. Phys. Chem.*, 2012, **31**, 1.
26 A. Li and H. Guo, *J. Chem. Phys.*, 2014, **140**, 224313.
27 H. Guo and B. Jiang, *Acc. Chem. Res.*, 2014, **47**, 3679.
28 H. Song, A. Li and H. Guo, *J. Phys. Chem. A*, 2016, **120**, 4742.
29 A. Li and H. Guo, *J. Phys. Chem. A*, 2014, **118**, 11168.
30 O. Martinez, S. G. Ard, A. Li, N. S. Shuman, H. Guo and A. A. Viggiano, *J. Chem. Phys.*, 2015, **143**, 114310.
31 S. G. Lias, J. E. Bartmess, J. F. Liebman, J. L. Holmes, R. D. Levin and W. G. Mallard, *J. Phys. Chem. Ref. Data*, 1988, **17**, Suppl. no. 1.
32 B. Jiang and H. Guo, *J. Chem. Phys.*, 2013, **139**, 054112.
33 J. Li, B. Jiang and H. Guo, *J. Chem. Phys.*, 2013, **139**, 204103.
34 D. Wang, *J. Chem. Phys.*, 2006, **124**, 201105.
35 M. Yang, *J. Chem. Phys.*, 2008, **129**, 064315.
36 H. Song and H. Guo, *J. Chem. Phys.*, 2014, **141**, 244311.
37 R. T. Pack, *J. Chem. Phys.*, 1974, **60**, 633.
38 P. McGuire and D. J. Kouri, *J. Chem. Phys.*, 1974, **60**, 2488.
39 J. A. Fleck, Jr., J. R. Morris and M. D. Feit, *Appl. Phys.*, 1976, **10**, 129.
40 W. L. Hase, R. J. Duchovic, X. Hu, A. Komornicki, K. F. Lim, D.-H. Lu, G. H. Peslherbe, K. N. Swamy, S. R. V. Linde, A. Varandas, H. Wang and R. J. Wolf, *Quantum Chem. Program Exch. Bull.*, 1996, **16**, 671.
41 W. L. Hase, *Encyclopedia of Computational Chemistry*, John Wiley & Sons, Ltd, 2002.
42 P. J. Chantry, *J. Chem. Phys.*, 1971, **55**, 2746.